Benha Journal of Applied Sciences (BJAS) **print: ISSN 2356–9751**
Vol. (7) Issue (12) (2022), (115-130) **online: ISSN 2356–976x**
http://bjas.journals.ekb.eg

Performance of composite cement containing Nano -ZnO subjected to elevated temperature

Mohamed Heikal[1], MY Nassar[1], S. Abd El-ALeem[2], A.M.El.Sharkawy[1], El-Hassan Desoki[1] and Sahar M Ibrahim[1]
[1]Chemistry, Dept., Faculty of Science, Benha Univ., Benha, Egypt
[2]Chemistry, Dept., Faculty of Science, Fayoum Univ., Fayoum, Egypt
E-mail: hassanelhelaly135@yahoo.com

ABSTRACT

The purpose of this article is studying the effect of physico-mechanical and fire-resistance of cement composite that contain ZnO-nanoparticles NZnO. ZnO-nanoparticles are prepared by combustion method. The composite cements are prepared with different amounts of NZnO 0.0, 0.1, 0.2, 0.4, 0.6 mass %. From one day to 90 days, the hydration kinetics' behavior was studied. After the specimens were subjected to thermal treatment at 200, 400, 600, 800 and 1000 ^{o}C, with a rate of heat 5^{o}C per minute for two hours, the composite cement pastes' thermal resistance was investigated. With a NZnO content of up to 0.6 mass percent, the compressive strength of OPC–NZnO cement pastes increased. The compressive strength of the thermally treated mixes with 0.6 % N-ZnO (NZTU4) is higher than that of the other mixes up to 1000 ^{o}C. It can be concluded that OPC–N ZnO pastes that contain 0.6 mass% NZnO have an optimal mix composition that has a better firing resistance than those of other pastes.

Keywords: Zinc oxide nanoparticles, cement, composite, transmission electron microscope Scanning electron microscope, x-ray diffraction

1. Introduction

New scientific fields called nanotechnology aim to comprehend and control matter at the nanoscale [1]. Unusual physical, chemical, and biological behavior can be seen in nanomaterials. An explosion of applications for nanomaterials in a variety of fields, including medicine, the environment and energy, chemistry, electronics, construction and automotive manufacturing, has resulted from the development of more effective nanoscale characterization methods. The microstructure of concrete, the physical and chemical reactions that take place in it, the improvement of these concretes, and the implementation of novel methods that make use of materials with nanoscale dimensions are those that are smaller than 100 nm. These nanomaterials are able to effectively fill the nano-pores that are present in the open vacant system of hydrated cement pastes. They also have the ability to increase the mechanical strength of pastes, mortar-fibers interfaces, and contact area's structural properties as well as concrete's durability [2-7]. The mechanical and durable properties of cement based materials containing nanoparticles have been the subject of several studies [8]. Nanoparticles were found to improve the mechanical properties of cement based materials, according to studies. New cement hydration accelerators are increasingly focusing on nanoparticles [9,10]. Due to their photocatalytic properties, ZnO nanoparticles have been used in self-cleaning concrete structures [11]. Nano-ZnO is an effective agent for enhancing the microstructure of cement pastes as well as a promoter of the pozzolanic reaction. It also serves as a filler to enhance the microstructure of cement [12]. As a result of addition of low concentrations of nano-ZnO with Portland cement, it enhances the mechanical properties and the microstructure of high strength cement pastes. This enhancement of pastes is due to an increase in particle packing and durability [13-17]. Due to the increased pozzolanic action, filling effect and improved the microstructure of cement pastes, the incorporation of Nano-ZnO increased the compressive strength and tensile strength of cement pastes [18]. Nano-ZnO accelerates the hydration reactions of cement phases because the particles fill the pores of the CSH by decreasing the crystal size of $Ca(OH)_2$ and acting as nucleation centers [19,20]. Additionally, NZnO's immediate reaction with cement pastes resulted in the formation of gels with high water retention capacities, which reduced the mix's workability [21]. The utilization of NZnO in concrete better the compressive strength, diminished of the porosity, because of adding ZnO prompted the utilization of portlandite ($Ca(OH)_2$) in the pozzolanic reaction, consequently enhancing the concrete microstructure to be strong and dense [22]. The effects of nano-materials in cement-based materials were the subject of several studies [13,23-31].

One of the major dangers that destroy building structures is fire. Exposing concrete to a higher temperature that has been thermally treated (for example, as a result of an accidental fire etc.) causes extensive deterioration and a variety of transformations and reactions, resulting in the gradual breaking of cementitious gel structure, decreased durability, an improved structural cracking and drying shrinkage [32].

Nano-modified cements were prepared by partially replacing OPC with 0.1, 0.2, 0.4, 0.6% by mass N-ZnO. The physico-chemical and mechanical properties of the produced nano-cements were examined by determining Wn%, FL%, bulk density and

compressive strength. XRD, DTA/TGA and SEM techniques were used to identify a few selected pastes. It was found that the compressive strength of the cement paste containing nano-ZnO particles was greater than that of a conventional cement paste. OPC-NZ pastes, which contain 0.6% by mass of NZnO, have an optimal mixture composition, which has good burning resistance than other pastes [33,34,35].

2. Materials and experimental techniques

The starting materials utilized were Type (I) ordinary Portland cement (OPC) and nano-zinc oxide (NZnO). Lafarge Cement Company, EGYPT, provided the ordinary Portland cement (OPC). Table 1 displays the chemical analysis. The Blaine surface area of OPC was 3350 cm^2/g.

Nano ZnO (NZ) were prepared by a gel combustion method. In this method we used zinc nitrate as oxidizing power and used fuel (tartaric acid+ urea) as reducing power. Zinc nitrate and fuel (tartaric acid+ urea) were dissolved in distilled water and homogenized on a magnetic stirrer. We controlled the pH using ammonia solution. The mixed solution was undergone heating at ca. 80 °C and stirring until the sol was turned into highly viscous gel. The temperature was then increased to ca. 300 °C, and this resulted in an exothermic combustion process. During this process, the fuel worked as a reducing agent and nitrate salts worked as oxidation agents. The combustion process brought about gray fine and intensively porous substance, which calcined at 600 °C ZnO nanoparticles were produced.

The crystallite size of NZnO which was prepared was 30.2 nm. As depicted in Figure. 1A and B, The mineralogical composition, crystal structure and micro-structure of NZnO were investigated using XRD and SEM. Table 2 depicts the characteristics of NZnO particles.

Table (1) Chemical composition of OPC, mass%.

SiO_2	Al_2O_3	Fe_2O_3	CaO	MgO	SO_3	Na_2O	K_2O	TiO_2	L.O.I	Total
20.22	5.02	3.44	63.21	1.77	2.57	0.39	0.25	0.51	2.75	100

Table (2) The properties of ZnO nanoparticles.

Formula	Purity(%)	Diameter(nm)	Crystal phase
ZnO	>99.9(wt%)	25±5	(hexagonal)

Table (3) Raw material characteristics.

Raw materials	Formulation	Molecular Weight(g\mol)	Purification(%)	Physical state
Zinc Nitrate	$Zn(NO_3)_2.6H_2O$	297.46	99	Solid
Tartaric acid	$C_4H_6O_6$	150	99	Solid
Urea	NH_2CONH_2	60	99	Solid

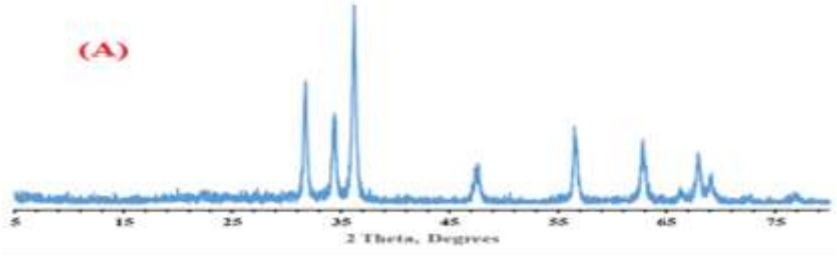

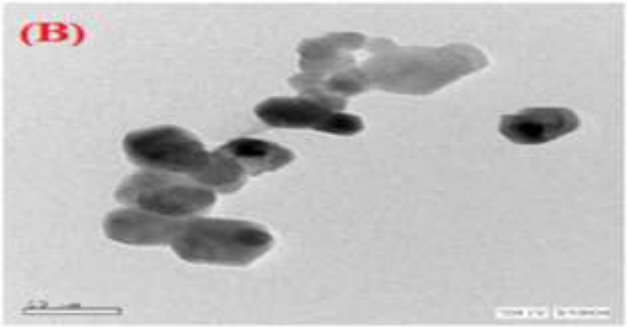

Fig. (1) Spectroscopic analytical techniques of prepared nano-ZnO (A) XRD, and (B) SEM

Table (4) Mix compositions of the prepared composite cements, mass%

Mix No.	OPC%	NZ%	W/C %
NZ0	100.0	0.0	0.27
NZ1	99.9	0.1	0.27
NZ2	99.8	0.2	0.27
NZ3	99.6	0.4	0.27
NZ4	99.4	0.6	0.27

A rotational mixer was used to mix the cement blends together. The procedure for mixing was as follows; The required water of standard consistency was used to stir the NZnO particles for one minute at a high speed (120 rpm). After the cement is added to the mixer, it is mixed for another 30 seconds at medium speed (80 rpm). The mixture was permitted to rest for 90 s and afterward mixed for one min at high speed. Table 4 displays the mix composition of the prepared cement blends.

The pastes were manually pressed into 2.45 × 2.45 × 2.45 cm cubic molds. Before being submerged in tab-water for 1, 3, 7, 28 and 90 days, the specimens were cured at a steady temperature 25±1 °C for the initial 24 hrs in 100% RH chamber. The hydration of cement pastes was stopped by pulverizing 10 g of representative sample in a beaker containing 1:1 (v/v) methanol-acetone mixture, and then mechanically stirred for one hour. The mixture was filtered through sintered glass G_4, after washing two times with the stopping solution and diethyl ether, then dried at 70 °C for two hours, then collected in polyethylene bags; sealed and stored in desiccators for analysis [36].

Using the following equation, the combined water content, or Wn, which represents the percentage of ignition loss in the pre-dried sample, was calculated:

$$Wn, \% = [(W_o - Wi)/Wi] \times 100$$

Where Wo is the dried sample's mass(g) before ignition and Wi is the ignited sample's mass (g) [37,38].

The hydrated cement pastes' free protlandite content can be determined. About 0.5 g of the sample is placed in small conical flask with 30 ml (glycerol: ethanol) solution (1:3) then we add strontium nitrate $Sr(NO_3)_2$ as indicator. The conical flask is placed on heater at 100°C for 10 min. the color of solution change to pink. The filtrate is titrated with a standard 0.1 N benzoic acid till a grey color appear (end point).

Before determining the specimens' compressive strength, the Bulk density was measured. Three similar cubes from same mix compositions and curing time were used for each measurement at least [39]. According to ASTM Designation:C-150, 2007, the compressive strength was determined [40]. A compressive strength machine of SEIDNER, Riedinger, Germany, with maximum capacity of 500 kN force was used to test a set of three cubes.

With the help of the XRD technique from BRUXER- Axs D8 ADVANCE A8 and the GERMANY Diffractometer, the crystalline phases of cement pastes were identified. The samples were finely ground to pass a 200- mesh sieve. Computer aided research of the pdf database took from the Joint Committee on Powder Diffraction Standards International Center for Diffraction Data (JCPDA-ICDD), 2001, confirmed that each sample had been identified.

The samples subjected to thermally treated temperature were demolded after 24 h, cured for 28 days under tap water, dried for 24 hrs at 105 °C, and then subjected to thermal treatment for 2 hrs at 200, 400, 600, 800 and 1000 °C with heating rate 5 °C /min, then cooled to room temperature in the furnace atmosphere. Bulk density and compressive strength of thermally treated cement pastes were determined after immersing the pastes overnight under Kerosene according to ISO-50/8, 1983.

DTA-50 Thermal Analyzer (Schimadzu Co., Tokyo, Japan) was used for thermal gravimetric analysis (TGA). Under nitrogen atmosphere, around 50 mg of a dried sample was utilized at rate of heat 20°C per minute.

The energy dispersive X-ray analyzer (EDX), Inspect S (FEI Company, Holland) was used to investigate the scanning electron microscope (SEM). The fractured composites' microstructure was examined with SEM at a Power zoom magnification up to 300,000$_\times$ and an accelerating voltage of 200–30 kV

3. Results and discussion

3.1. Hydration behavior of composite cement pastes

3.1.1 Compressive strength

Figure 2 depicts the effect of NZ contents on the compressive strength of hydrated cement pastes that have been hydrated for up to 90 days. Due to the continuous hydration and formation of successive amounts of hydrated products (C-S-H, C-A-H, C-A-S-H and Portlandite), the compressive strength of all hydrated cement pastes increases with the curing time. These hydrates settled into the open pores that were available, resulting in a closed compact structure. The compressive strength of OPC-NZnO cement pastes increase with NZnO content up to 0.6% (NZTU4) mix

than those of OPC paste. There are two reasons why NZ increases the compressive strength of hardened cement pastes. The first factor, NZnO acts as activator to facilitate the pozzolanic reaction with CH that is released during cement hydration to form additional hydrated products of CSH, CAH and CASH. The second factor is due to NZnO improves the interfacial transition zone and acts as a filler and packing factor into interstitial spaces [41-44]. The inclusion of 0.6 mass% NZnO increases the compressive strength from 264 to 452 Kg/cm^2 after 1 day of hydration, whereas, the compressive strength increases from 831 to 1021 Kg/cm^2 at 90 days.

3.1.2. Bulk density

Figur. 3 shows the values of the bulk density of NZnO-OPC cement pastes that have been hydrated for up to 90 days. Increasing the curing time from one day to 90 days the bulk density values of OPC-NZnO composite cement pastes increases up to 0.6 mass%. The bulk density of NZTU4 mix is higher than those of other composite cement pastes from one day up to 90 days; this is due to the higher pozzolanic activity of NZnO particles. However, strength values of NZTU1 mix with 0.1 mass% of NZ are lower than those of neat OPC pastes for up to 90 days. NZnO increases the pozzolanic activity, resulting in an excessive increase in the formation of crystalline CSH hydrates; these hydrates, which function as nano-fillers, increase the total contents of binding centers and reduce the total porosity [45-46].

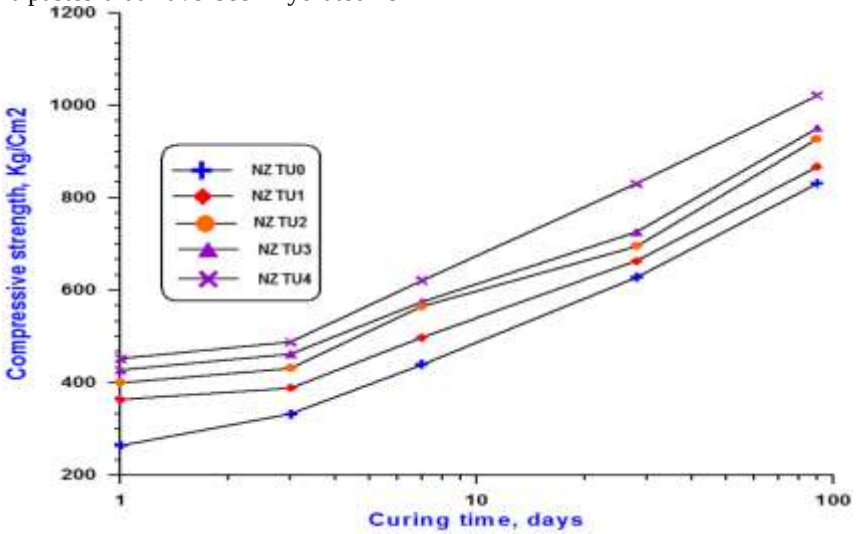

Fig. (2) Compressive strength of the hydrated NZnO–OPC cement pastes

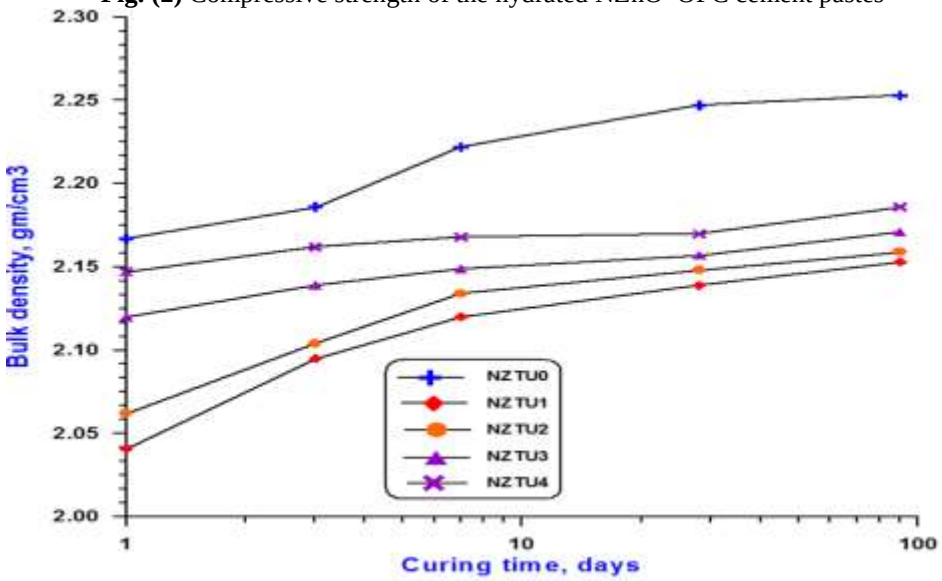

Fig. (3) Bulk density of NZ–OPC cement pastes as a function of curing time

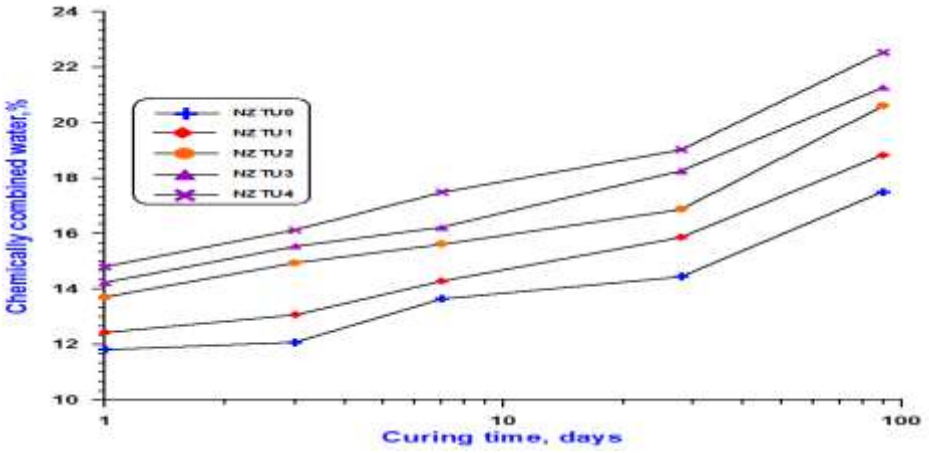

Fig. (4) Chemically combined water contents of hydrated ZnO-cement pastes up to 90 days

3.1.3. Chemically combined water contents

Figure 4 depicts Chemically combined water contents of hydrated ZnO-cement pastes up to 90 days. The amounts of chemically combined water can be used to determine the level of hydration. Due to the continuous of the hydration, the chemically combined water contents of all hydrated NZnO-cement pastes rise with increasing curing age, resulting in the precipitation of larger quantities of hydrated products in the hardened cement pastes' accessible open pores. When compared to the values of neat-OPC paste for up to 90 days, the chemically combined water contents' values rise with rising the content of NZnO to 0.6 mass, indicating an increase in hydration reaction rate. Additionally, the cement's hydration was sped up by the high activity and nucleating effect of NZnO particles. At all curing ages, the composite cement (NZTU4) mix with 0.6 mass% of NZnO has the highest values of chemically combined water contents.

3.1.2 Free protlandite contents

Figure 5 depicts the free lime contents (FL%) of NZnO-cement pastes with varying NZnO percentages for up to 90 days. The results indicated that the neat-OPC paste's free protlandite values rise to 90 days; The hydration continuously of the main phases of cement (C_3S and βC_2S) is the cause of the rise in free protlandite values for up to 90 days. Due to the higher pozzolanic activity of NZ or the rate of consumption is higher than that of liberation, the free lime content of a composite containing OPC–NZnO decreases for up to 90 days. NZ is extremely reactive because it forms CSH condensed gel through pozzolanic reaction and its high special surface. The free lime contents of OPC-NZ composite cement pastes decrease with NZnO content, reaching a maximum of 0.6 mass%. In addition, the amount of free protlandite content in composite cement pastes decreases significantly as the percentage of NZnO replacement level rises.

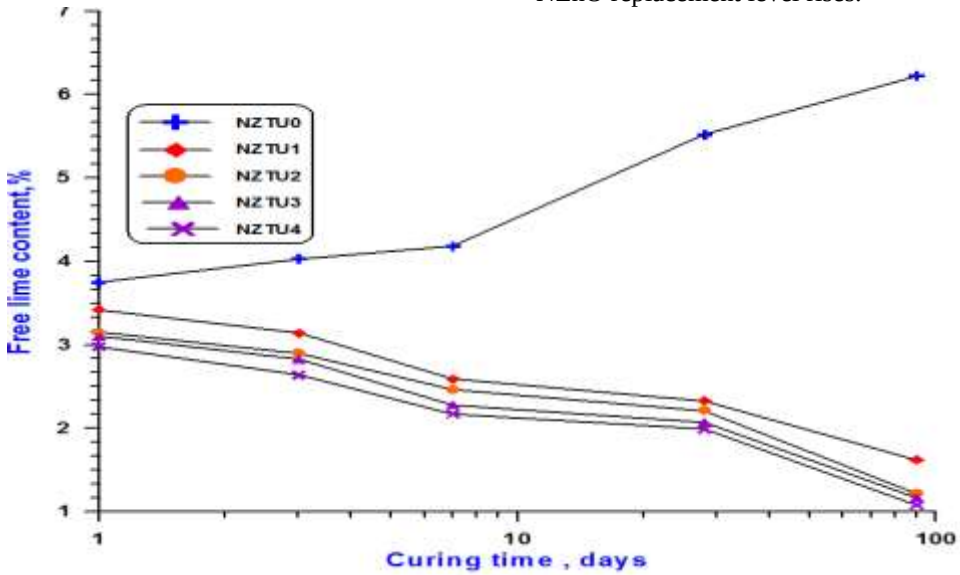

Fig. (5) contents of free protlandite in hydrated NZnO cement pastes that can cure for up to 90 days.

3.1.3 Total porosity contents

Figure 6 shows the variations of total porosity (TP) of composite cement pastes with 0.1%, 0.2%,0.4%,0.6% NZnO hydrated for up to 90 days. The results showed that the porosity content of OPC paste decreased with curing time for up to 90 days. This is because
the hydration reaction of the cement phases continued, resulting in an excessive amounts of the ore-dense structure of hydrates. Cement-pastes containing 0.6 % NZnO (NZTU4) mix have a lower TP than neat-OPC and the other-mixes. The results concluded that physico-mechanical properties, namely CS, chemically combined water, TP, and BD are in good agreement with each other. Where the physico-mechanical properties show an increase in the values of CS, chemically combined water, and BD from one days up to 90-days.

3.1.4. XRD diffraction patterns:

Figure 7A-C represented XRD patterns of OPC and NZnO-composite cement hydrated at 28 days and 90 days. Figure7A illustrates the XRD diffraction patterns of OPC cement paste (NZTU0) mix at 28, 90 days. The diffraction patterns showed the presence of diffraction lines corresponding to hydrated and anhydrated cement phases namely, C-H, βC_2S, C_3S, $CaCO_3$ (C-C) and CSH gel. The XRD diffraction patterns showed the peak intensity of CSH, C-H, and CC increased with curing time at 90 days. So the compressive strength value of OPC paste (NZTU0) at 90 days more than 28 days.

Figure 7B shows the XRD diffractograms of the hardened mixes NZTU0, NZTU1, NZTU2, NZTU3 and NZTU4 hydrated for 28 days. Mix NZTU4 exhibit lower intensities of diffraction lines corresponding to C-H in comparison with those of NZTU2. Therefore, the rate of lime consumption and formation of CSH increases in the presence of mix NZTU4. This result confirms the increase of compressive strength and bulk density as shown above in Figures 2 and 3.

Figure 7C illustrates the XRD diffraction patterns of OPC-NZnO composite cement paste containing 0.6 mass% NZnO (NZTU4) mix hydrated up to 90 days. The diffraction patterns showed the presence of diffraction lines corresponding to hydrated and anhydrated cement phases namely, CH, β-C_2S, C_3S, $CaCO_3$ (CC) and C–S–H. The diffraction peak intensity corresponding to CSH increased, whereas intensities of the diffraction peaks corresponding CH decreased with curing time due to the pozzolanic reaction with NZ, leading to the consumption of CH and formation of additional C–S–H, C–A–H and C–A–S–H hydrated products. So the compressive strength values of mix containing 0.6mass %NZnO (NZTU4) mix increased with curing time.

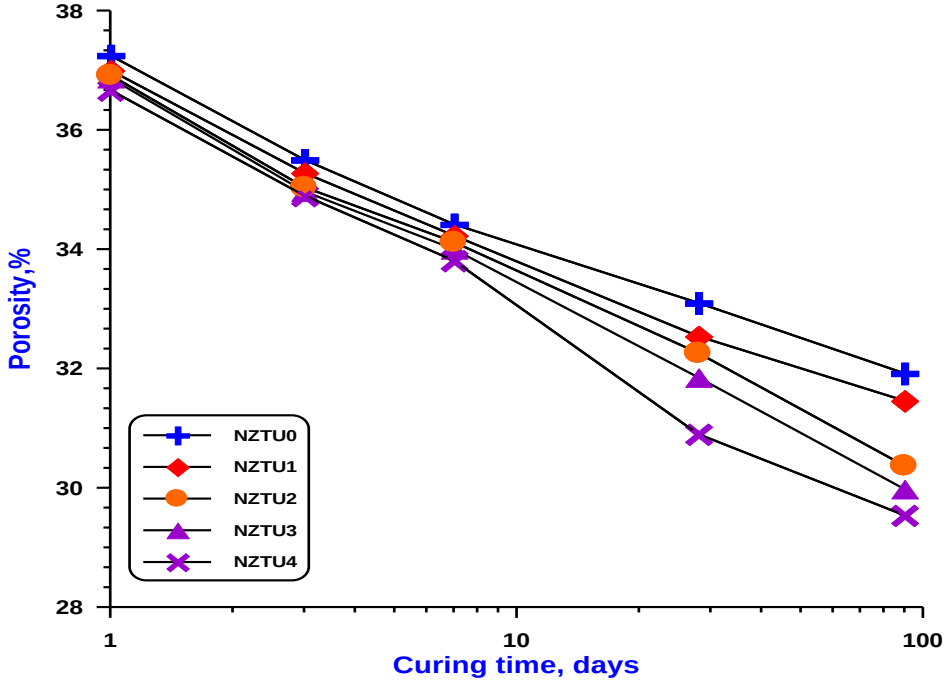

Fig. (6) Porosity contents of hydrated composite cement pastes containing NZ with curing time up to 90 days.

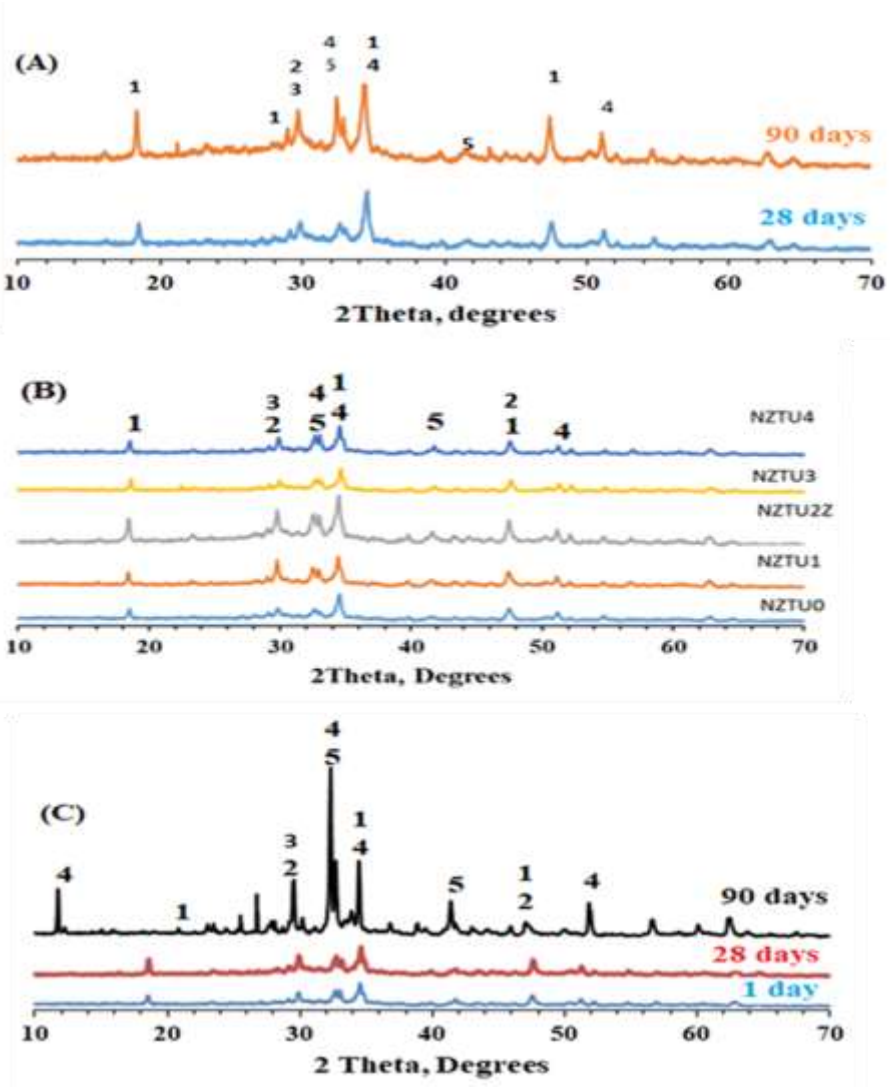

Fig. (7) XRD patterns of hardened OPC-NZnO composite cement pastes; (A) NZTU0 at 28 days and 90 days; (B) mixes NZTU0, NZTU1, NZTU2, NZTU3, and NZTU4; (C) mix NZTU4 at 1, 28, and 90 days.C-H = 1; C-C= 2; CSH = 3; β-C_2S = 4; C_3S = 5

3.1.5. Scanning electron microscopy.

Figure 8 (A, B) represents the SEM images of OPC(NZTU0) mix at 28 and 90 days, the micrograph represented the formation of CSH and ettringite hydrated products at 28 and 90 days.

SEM micrograph reveals the formation of much denser microstructure at 90 days .The structure was found to be a compact dense matrix.

Figure 9 (A-D) represents the SEM images of the hardened mixes NZTU1, NZTU2, NZTU3 and NZTU4 hydrated for 28 days. The micrograph represented formation of CSH, CAH and CASH and these compounds are much denser microstructure at NZTU4.

Figure 10A ,B ,C. represents the SEM micrographs of OPC-NZnO composite cement paste containing 0.6 mass% NZnO (NZTU4) hydrated at 1, 28, 90 days. The micrograph represents the formation of CSH, CAH and CASH. These hydrated products showed more progress and intensified at 28and 90 days.

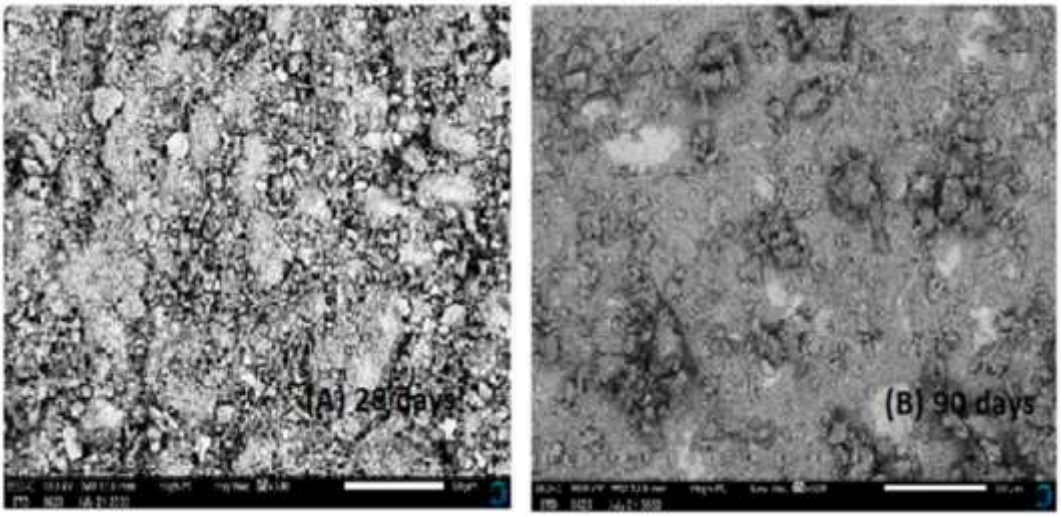

Fig. (8) SEM of NZTU0 mix cured for: (A) 28 days; (B) 90 days

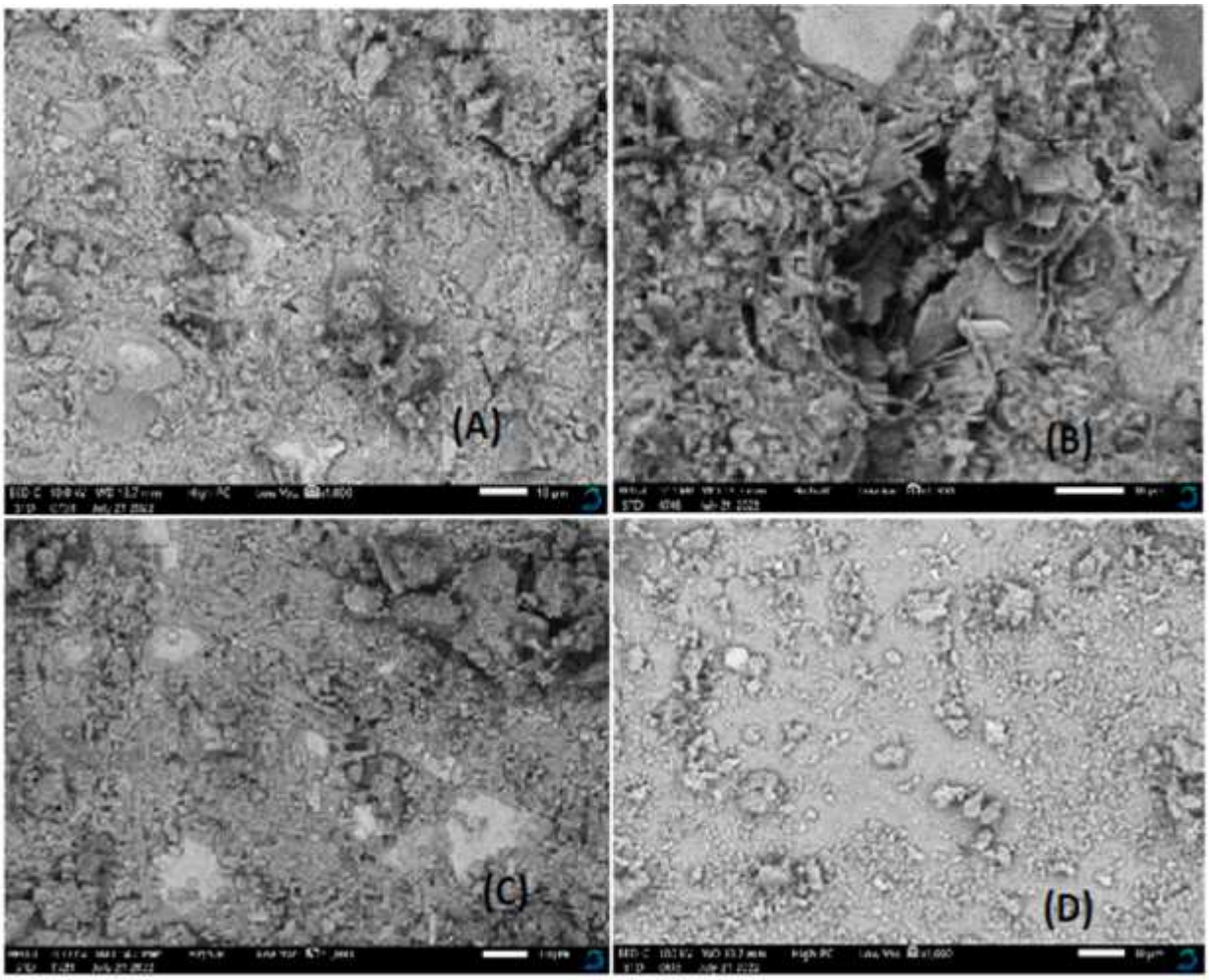

Fig. (9) SEM of NZnO-composite pastes at 28 days: (A) NZTU1 mix; (B) NZTU2 mix; (C) NZTU3 mix; (D) NZTU4 mix

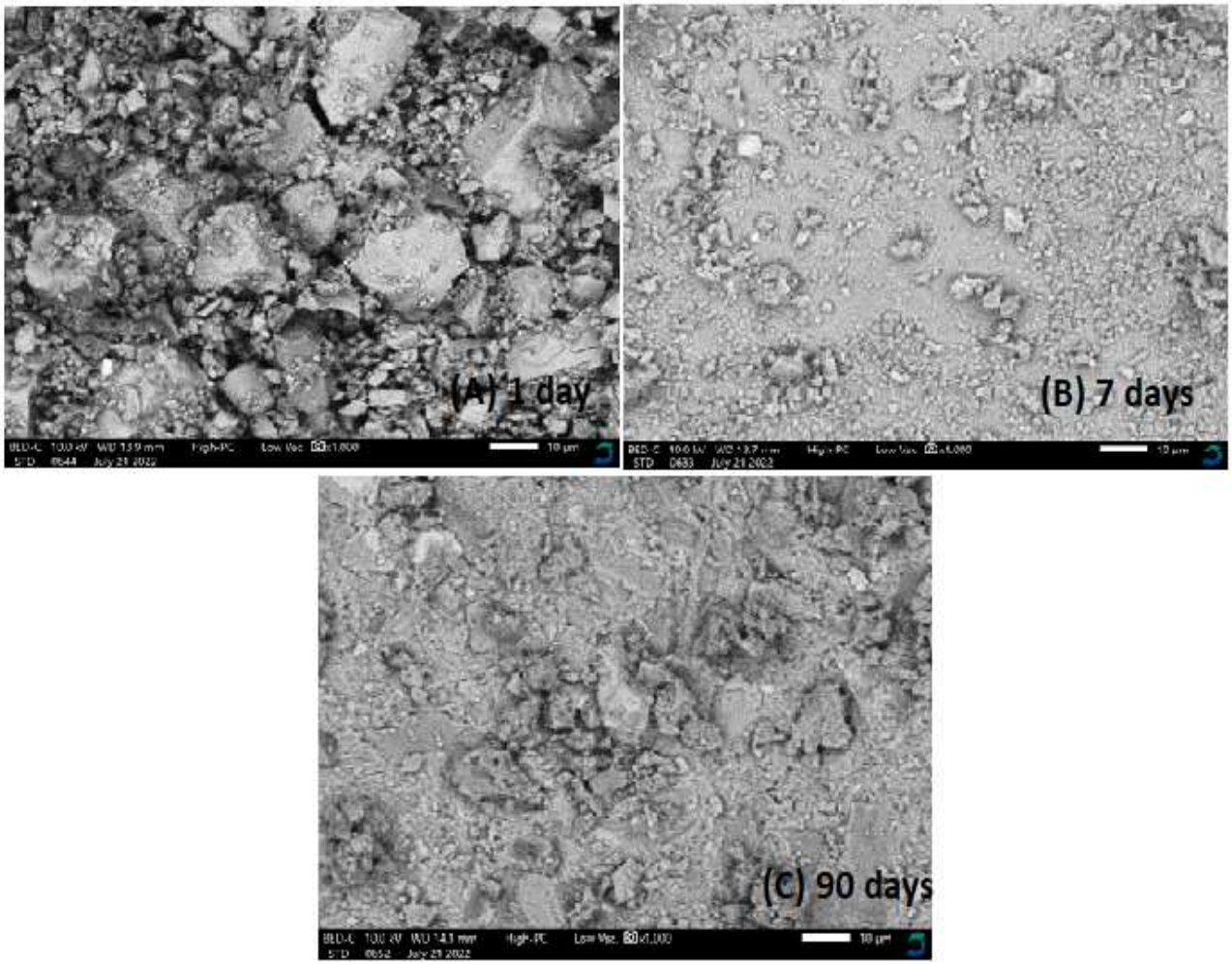

Fig. (10) SEM of NZTU4 mix cured for: (A) 1 day; (B) 28 days; (C) 90 days

3.2. Behavior of composite cement pastes at elevated temperature

3.2.1 Weight loss

Fig. 11 depicts the weight loss of the hardened OPC-NZ composite cement pastes at temperatures up to 1000 °C. Due to the chemical processes stimulated by treatment temperature in the various phases of cement pastes, the weight loss increases with temperature. At 105 °C, the evaporable water was removed, and around 200 °C, sulphoaluminate hydrates, CSH and CAH were partially decomposed. Gehlenite hydrate (C_2ASH_8) decomposition at temperatures above 200 °C. C-H was dehydroxylated between 400-550 °C. Between 650 and 800 °C, the decarbonation of calcium carbonate occurred. The results indicated that elimination of adsorbed, free, bound water of cement pastes significantly rises weight loss to 250°C. Up to 1000°C, the weight loss slightly increased with temperature. This is because of the dehydration of CH at temperatures between 400-500 °C and the breakdown of some hydrated products like C–S–H, calcium sulphoaluminate, and gehlenite like hydrate (C_2ASH_8). As the substitution of OPC increased up to 0.6% NZ, the weight loss of cement pastes up to 1000 °C, this is due to higher consumption of liberated CH with the formation of additional hydrarated products, which fill the open pores forming interlocking close and compact nanostructure [39,47].

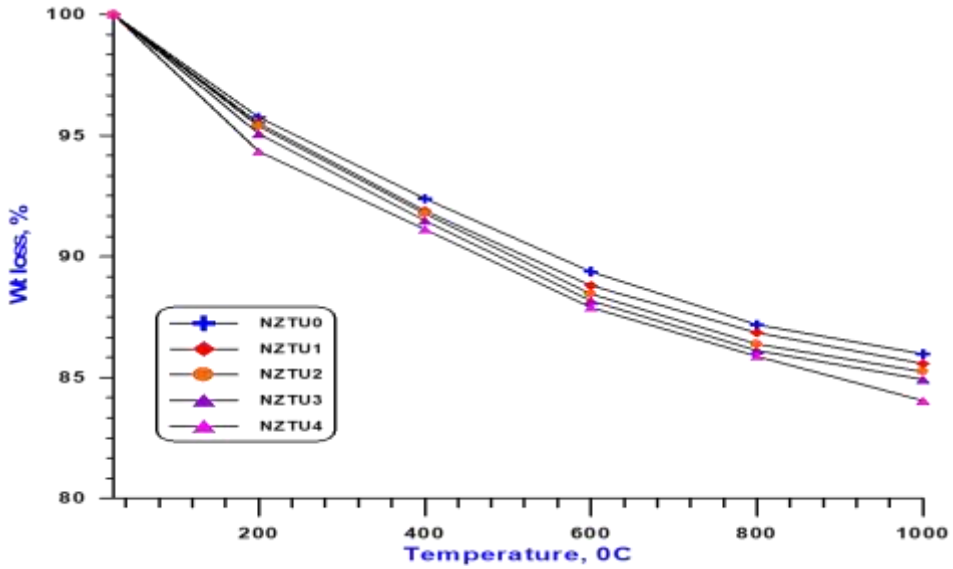

Fig. (11) Weight loss of NZnO- containing hardened composite cement pastes at temperatures to 1000°C

3.2.2. Compressive strength

Figure 12 depicts graphically the variations in compressive strength of the hardened OPC–NZ composite cement pastes as a function of treatment temperature up to 1000 °C. Up to 400 °C of thermal treatment raises the compressive strength [39,48,49]. At all temperatures of thermal treatment up to 1000°C, the compressive strength of 0.6 NZ is at its highest. Enhancing the hydration of unhydrated cement clinker results in an increase in the compressive strength of OPC–NZnO composite [50]. The high temperature result in flow of steam from removal of physically, capillary, adsorbed and bound water in cement pastes that create hydration products due to internal autoclaving reaction ,in addition to enhancement of pozzolanic reaction of NZ with C-H to form extra CSH with high strength [39,51,52]. At 600–1000 °C, the compressive strength decreases, possibly as a result of the decomposition of cementitious materials like C–S–H. These hydrates undergo thermal treatment at temperatures to 1000°C, resulting in the formation of wallastonite crystalline phases and a crystalline structure resembling that of C_2S. The pore system is opened by these crystalline phases, resulting in an increase in porosity and a decreases in compressive strength. It can be included that NZ with a mass of 0.6% is more resistant to fire than any other composite cement pastes.

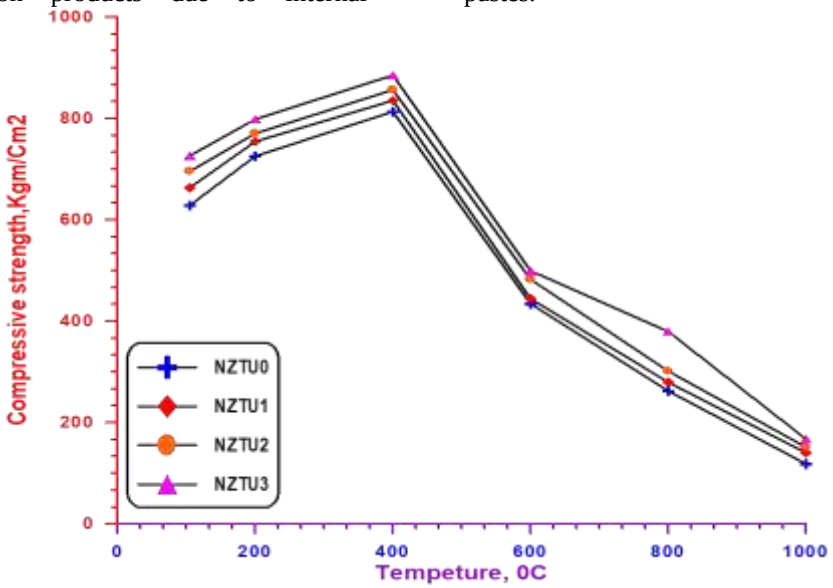

Fig. (12) Compressive strength of NZ- containing hardened composite cement pastes at temperatures to 1000°C

3.2.3. Bulk density

Figure 13 depicts bulk density of NZ-containing hardened composite cement pastes at temperatures to 1000°C.The variations of bulk density of thermally treated OPC-NZ pastes occur in different steps. The self-internal autoclaving reaction that results in the formation of additional hydration products from an anhydrous cement and the pozzolanic reaction of NZnO with CH that results in the formation of additional C-A-H, CZH and C-A-S-H hydrated products both increase the bulk density at the first step up to 200 °C. The elimination of adsorbed, free, chemically combined water of calcium aluminosilicate hydrates, CAH and CSH results in a bulk density decreases of up to 400 °C during the second step. The decomposition of calcium carbonate into CaO and CO_2 results in an increase in the bulk density values between 400 °C and 600 °C (the third step). Up to a temperature of 1000 °C, the bulk density of the (NZTU4) mix is higher. This is because the the hydration products from the cement clinker phases have higher values. the pore size distribution were strongly losses and coarsening because of raising temperature above 600–1000 °C [47,53,54]. this results in the formation of a denser structure and the shrinkage that goes along with it, consequently, both the total porosity and bulk density increase. The dense mater produced by sintering from solid state results in an increase in bulk density.

3.2.4. Total porosity

Figure 14 depicts the OPC–NZ composite cement pastes' total porosity as a function of treatment temperature. The temperature of thermal treatment increases the hydration of un-hydrated cement phases and the reaction of NZnO with C-H to create extra hydration products that fill up the existing pores, both of which reduce total porosity up to 200 °C [53,55-57]. For all cement pastes, the total porosity rises abruptly with treatment of temperature from 200°C to 1000°C because of the creation of microcracks and rise of crystallinity degree of the hydrates that are formed, which results in a kind of opening in the pore system of the cement pastes [55,56]. NZnO content decreases total porosity; this is because CH is used to create more hydration products. Additionally, a significant increase of micro-cracks causes a sharp increase in porosity between 600 and 800 °C. The degredation of C-H at 600°C increase porosity. Because of the degredation of some carbonated CSH as well as the other hydration products, the porosity increases after 600°C to 1000°C. Sintering caused significant coarsening and loss of strength at exposed temperatures up to 1000 °C. The distribution of pore size is affected by the rising temperature. The increase in total porosity can be linked to the decrease in compressive strength.

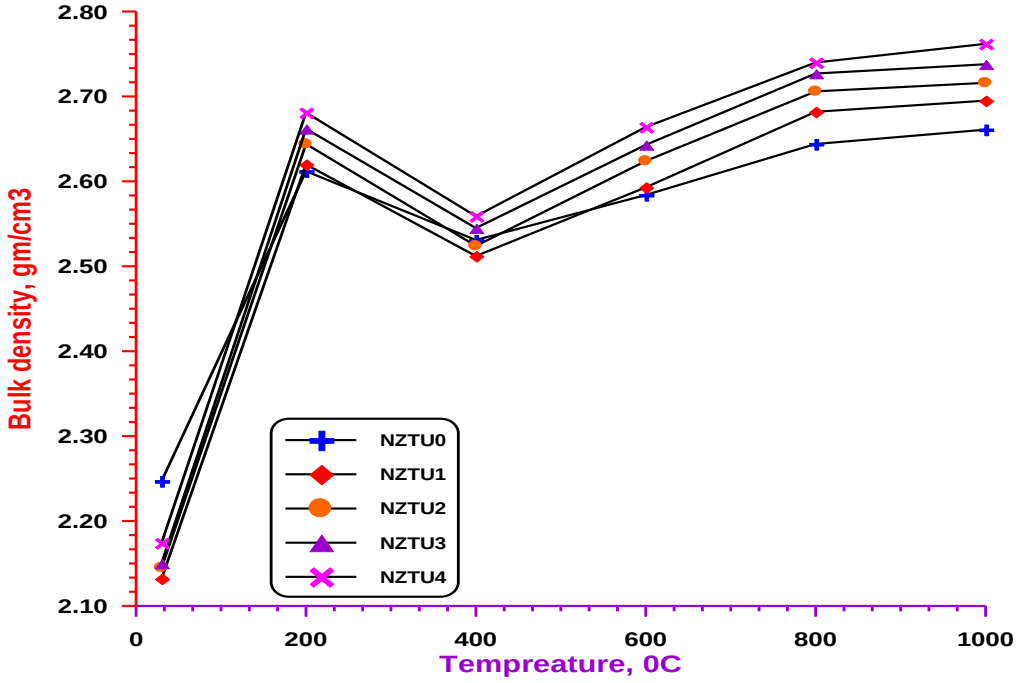

Fig. (13) Bulk density of NZ-containing hardened composite cement pastes at temperatures to 1000°C.

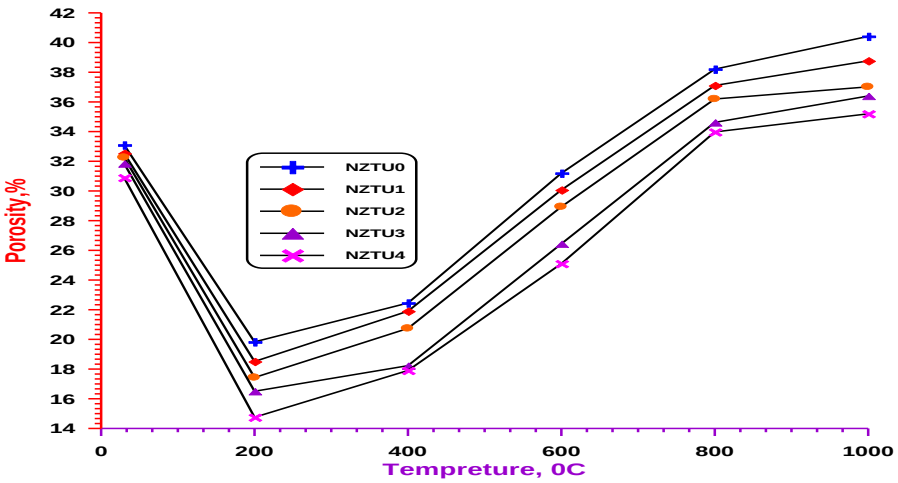

Fig. (14) Total porosity of NZnO- containing hardened composite cement pastes at temperatures to 1000°C.

3.1.4. XRD diffraction patterns:

Figure 15A shows the diffraction lines of mixes NZTU0, NZTU2 and NZTU4 containing 0, 0.2, and 0.6 mass% NZnO hydrated at 28 days. X-ray diffractograms show the presence of C-H, βC_2S, C_3S, CC, and CSH. The peak height of CSH, and C-H phase corresponding to 0.6 mass% NZnO decreases than those of peak containing 0 and 0.2 % NZnO.

Figure 15B shows XRD diffraction patterns of NZTU4 mix contains 0.6 mass% NZnO at 400,600, and1000 °C. XRD diffraction patterns of 0.6% NZnO (NZTU4 mix) at 400 °C demonstrates the main phases as CSH gel, unhydrated C3S ,and β-C2S, C-H and C-C. The diffraction lines because of C-H, demonstrated that the intensities of diffraction lines corresponding to C-H of mix NZTU4 at 400 °C are more than the intensities of diffraction lines corresponding to CH at 600 °C are more than the intensities of diffraction lines corresponding to CH at 1000 °C. Moreover, the intensity of diffraction lines corresponding to CSH at 400 °C are more than that of C-S-H at 600 °C and at 1000 °C .The peak intensity of (C_3S and β-C_2S) at 400 less than 600 °C less than 1000 °C. It was concluded that NZnO at 400 °C has more hydration products than at 600 and 1000 °C. There is an overlap between the lines of C-C and the lines of CSH.

The intensity of C-C peak that was removed at 1000°C because of partial decomposition into CaO. At 1000°C CSH has completely disappeared because of the change to crystalline anhydrous calcium silicate phases.

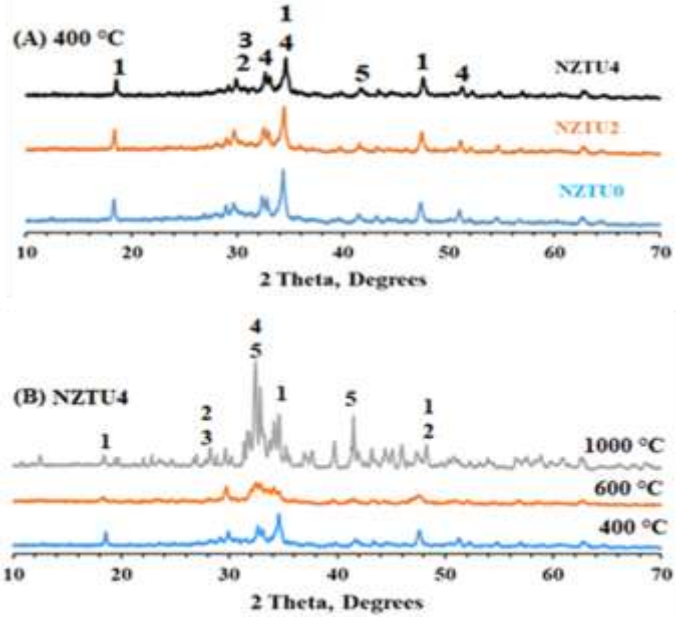

Fig. (15) XRD diffraction patterns of OPC-NZnO composite cement pastes at temperatures up to 1000 ^{O} C; (A) mixes NZTU0, NZTU2, and NZTU4; (B) mix NZTU4 at 400, 600, and 1000 ^{O} C; CH = 1; CC 2; C-S-H =3; β-C2S = 4; C3S = 5

3.1.5. Scanning electron microscopy

Figure 16 (A-C) represented SEM micrographs of mixes NZTU0,NZTU2 and NZTU4 at 400°C. The micrograph displays a combination of CSH,CAH,CSAH. These compounds are a denser at NZTU4.

Figure 17 (A-C) represents SEM micrographs of mix NZTU4 at 400,600, and1000 °C

A combination CSH and hexagonal sheet of $Ca(OH)_2$ with a porous-structure morphology is displayed in the micrograph. The large amount of hydrates are decomposed because of increasing of the thermally treated temperature to 1000 °C, these hydrates leads to open the pore matrix ,so compressive strength decreased at 1000 °C

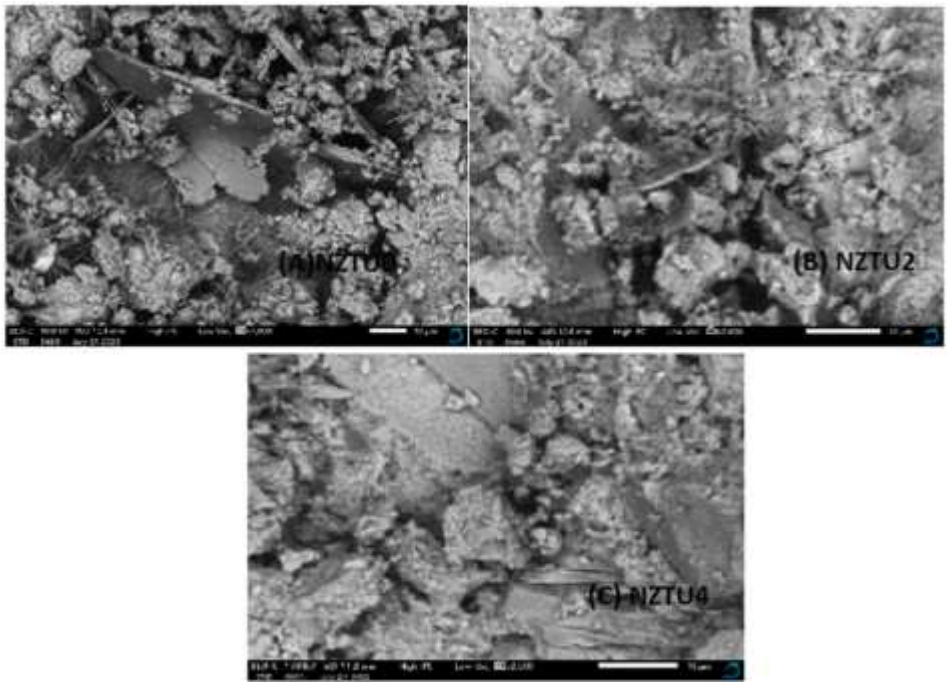

Fig. (16) SEM of NZnO composite cement pastes treated at 400 °C (A) NZTU0 ; (B) NZTU2 ; (C) NZTU4

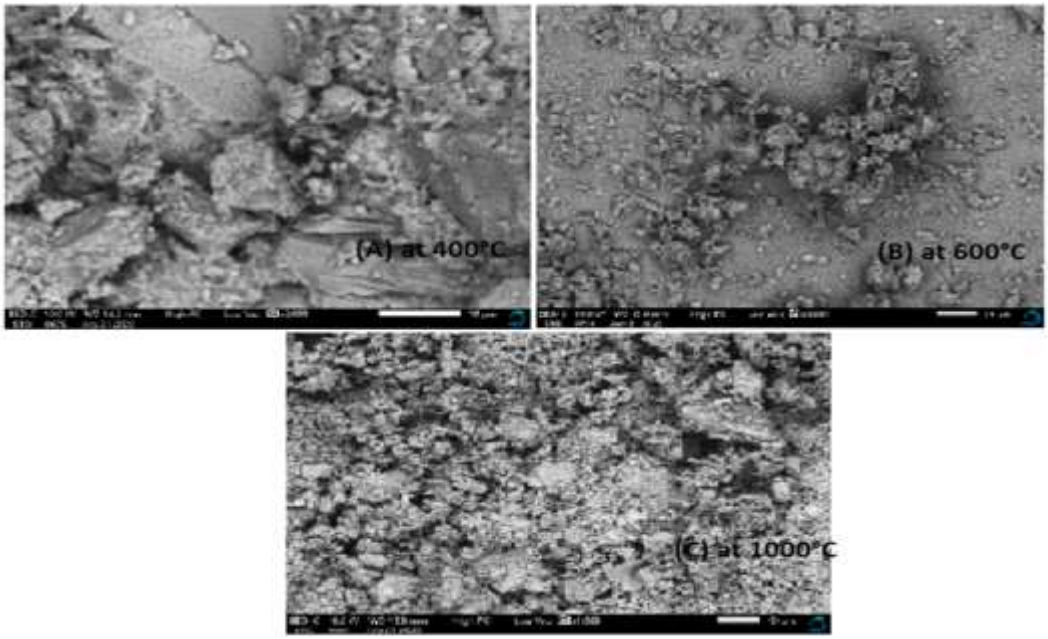

Fig. (17) SEM of NZTU4 treated at: (A) 400 °C ; (B) 600 °C ; (C) 1000 °C

4. Conclusions

From the above findings it can concluded that:

1. The compressive strength of OPC–NZ cement pastes increase with NZnO content up to 0.6%. 0.6 mass% NZnO nano-particles is appropriate amount, which improves the compressive strength of OPC paste with 29.12%
2. Chemically combined water contents increased by up to 0.6 mass% as NZnO content increased. At all curing ages, the OPC-NZ composite cement with 0.6 mass% NZ (NZTU4) has the highest chemically combined water contents.
3. OPC–NZ's free lime content decreased for up to 90 days.
4. Because of increasing pozzolanic activity necessary to generate additional CSH hydrated products, mixtures containing OPC-NZ exhibit an increase in ignition loss between 200 and 400 ^{O}C.
5. With cement pastes containing 0.1, 0.2, 0.4, and 0.6% NZnO, the compressive strength increases by 12.65, 21.9, 23.16, and 25.94 % as the thermally treated temperature rises from 25 °C to 450 °C, respectively.
6. The compressive strength of 0.6% NZ was highest at all temperatures of thermal treatment up to 1000 °C. It can be concluded that 0.6mass% NZ has a higher resistance to fire than all composite cement pastes.
7. Bulk density values are highest in mixes (NZTU3 and NZTU4).
8. The data demonstrated that, up to a temperature of 1000 °C, the total porosity of (NZTU3 and NZTU4) mixes is lower than that of other composite cement pastes.

References

[1] Zhu, W., Bartos, P.J., & Porro, A. (2004). Application of nanotechnology in construction. Materials and structures, 37(9), 649–658.

[2] Wiesner, M. R., & Bottero, J. Y. (2017). Environmental nanotechnology: applications and impacts of nanomaterials. McGraw-Hill Education

[3] Qing, Y., Zenan, Z., Deyu, K., &Rongshen, C. (2007). Influence of nano-SiO_2 addition on properties of hardened cement paste as compared with silica fume. Construction and building materials, 21(3), 539–545.

[4] Li, G. (2004). Properties of high-volume fly ash concrete incorporating nano-SiO_2. Cement and Concrete research, 34(6), 1043–1049.

[5] Aly, M., Hashmi, M. S. J., Olabi, A.G., Messeiry, M., Abadir, E. F., & Hussain, A.I. (2012). Effect of colloidal nano-silica on the mechanical and physical behavior of waste-glass cement mortar. Materials & Design ,33, 127–135.

[6] Nazari, A., & Riahi, S. (2011). RETRACTED: The effects of SiO_2 nanoparticles on physical and mechanical properties of high strength compacting concrete.

[7] Amiri, B., Bahari, A., Nik, A. S., Nik, A. S., &Movahedi, N. S. (2012). Use of AFM technique to study the nano-silica effects in concrete mixture. Indian Journal of Science and Technology, 5(2), 2055–2059.

[8] Sobolev, K., Flores, I., Hermosillo, R., & Torres-Martınez, L. M. (2006). Nanomaterials and nanotechnology for high performance cement composites. Proceedings of ACI Session on nanotechnology of concrete: recent developments and future perspectives, 7, 93-120.

[9] Mukhopadhyay, A.K. (2011). Next generation nano-based concrete construction products: a review. Nanotechnology in civil infrastructure, 207–223.

[10] Rashad, A.M. (2013) .A synopsis about the effect of nano-Al_2O_3, nano-Fe_2O_3, nano-Fe_3O_4 and nano-clay on some properties of cementitious materials – A short guide for Civil Engineer. Materials & Design (1980-2015), 52, 143–157.

[11] Kenanakis, G., Vernardou, D., & Katsarakis, N. (2012). Light-induced self-cleaning Properties of ZnO nanowires grown at low temperatures. Applied Catalysis A: General, 411, 7-14.

[12] Choolaei, M., Rashidi, A. M., Ardjmand, M., Yadegari, A., & Soltanian, H. (2012). The effect of nanosilica on the physical properties of oil well cement. Materials Science and Engineering: A, 538, 288–294.

[13] Qing, Y., Zenan, Z., Deyu, K., & Rongshen, C. (2007). Influence of nano-SiO_2 addition on properties of hardened cement paste as compared with silica fume. Construction and building materials, 21(3), 539–545.

[14] Stefanidou, M., & Papayiann, I. (2012). Influence of nano-SiO_2 on the Portland cement pastes. Composites Part B: Engineering, 43(6), 2706–2710.

[15] Tobon, J. I., Restrepo, O. J., &Paya, J. (2010). Comparative analysis of performance of Portland cement blended with nanosiliaca and silica fume. Dyna, 77(163), 37–46.

[16] Ji, T. (2005). Preliminary study on the water permeability and microstructure of concrete incorporating nano-SiO_2. Cement and concrete Research, 35(10), 1943–1947.

[17] Gaitero, J. J., Campillo, I., & Guerrero, A. (2008). Reduction of the calcium leaching rate of cement paste by addition of silica nanoparticles. Cement and concrete research, 38(8–9), 1112–1118.

[18] Jo, B. W., Kim, C. H., Tae, G. H., & Park, J. B. (2007). Characteristics of cement mortar with nano-SiO_2 particles. Construction and building materials, 21(6), 1351–1355.

[19] Sanchez, F., & Sobolev, K. (2010). Nanotechnology in concrete – a review. Construction and building materials, 24(11), 2060–2071.

[20] Pacheco-Torgal, F., Miraldo, S., Ding, Y., & Labrincha, J. A. (2013). Targeting HPC with the help of nanoparticles: an overview. Construction and Building Materials, 38, 365–370.

[21] Berra, M., Carassiti, F., Mangialardi, T., Paolini, A. E., & Sebastiani, M. (2012). Effects of nanosilica addition on workability and compressive strength of Portland cement pastes. Construction and Building Materials, 35, 666–675.

[22] Said, A. M., Zeidan, M. S., Bassuoni, M. T., & Tian, Y. (2012). Properties of concrete incorporating nano-silica. Construction and building materials, 36, 838–844.

[23] Lin, K. L., Chang, W. C., Lin, D. F., Luo, H. L., & Tsai, M. C. (2008) Effects of nano-SiO_2 and different ash particle sizes on sludge ash–cement mortar. Journal of environmental management, 88(4), 708–714.

[24] Li, H., Xiao, H. G., Yuan, J., & Ou, J. (2004). Microstructure of cement mortar with nanoparticles. Composites part B: engineering, 35(2), 185–189.

[25] Li, G. (2004). Properties of high-volume fly ash concrete incorporating nano-SiO_2. Cement and concrete research, 34(6), 1043–1049.

[26] Bjornstrom, J., Martinelli, A., Matic, A., Borjesson, L., & Panas, I. (2004). Accelerating effects of colloidal nano-silica for beneficial calcium–silicate–hydrate formation in cement. Chemical physics letters, 392(1–3), 242–248.

[27] Shih, J. Y., Chang, T. P., & Hsiao, T. C. (2006). Effect of nanosilica on characterization of Portland cement composite. Materials Science and Engineering: A, 424(1-2), 266–274.

[28] Chen, J., & Poon, C. S. (2009). Photocatalytic construction and building materials: From fundamentals to applications. Building and environment, 44(9), 1899–1906.

[29] Ruot, B., Plassais, A., Olive, F., Guillot, L., &Bonafous, L. (2009). TiO2-containing cement pastes and mortars: Measurements of the photocatalytic efficiency using a rhodamine B-based colourimetric test. Solar Energy, 83(10), 1794–1801.

[30] Hassan, M. M., Dylla, H., Mohammad, L.N., & Rupnow, T. (2010). Evaluation of the durability of titanium dioxide photocatalyst coating for concrete pavement. Construction and building materials, 24(8), 1456–1461.

[31] Husken, G., Hunger, M., & Brouwers, H. J. H. (2009). Experimental study of photocatalytic concrete products for air purification. Building and environment, 44(12), 2463–2474.

[32] Andic, O., Copurog˘lu, O., & Ramyar, k. (2008). Effect of high temperature on mechanical and microstructural properties of cement mortar. In 11th International conference on durability of building materials and components, Istanbul (pp. 527-533).

[33] Gawlicki, M., & Czamarska, D. (1992). Effect of ZnO on the hydration of Portland cement. Journal of Thermal Analysis and Calorimetry, 38(9), 2157-2161.

[34] Ataie, F. F., Juenger, M. C., Taylor-Lange, S. C., & Riding, K. A. (2015) Comparison of the retarding mechanisms of zinc oxide and sucrose on cement hydration and interactions with supplementary cementitious materials. Cement and Concrete Research, 72, 128-136.

[35] Nochaiya, T., Sekine, Y., Choopun, S., & Chaipanich, A. (2015). Microstructure, characterizations, functionality and compressive strength of cement-based materials using zinc oxide nanoparticles as an additive. Journal of Alloys and Compounds, 630, 1-10 .

[36] Aziz, M. A. E., Aleem, S. A. E., & Heikal, M. (2012). Physico-chemical and mechanical characteristics of pozzolanic cement pastes and mortars hydrated at different curing temperatures. Construction and Building Materials, 26(1), 310–316.

[37] El-Didamony, H., Aiad, I., Heikal, M., & Al-Masry, S. (2014). Impact of delayed addition time of SNF condensate on the fire resistance and durability of SRC–SF composite cement pastes. Construction and Building Materials, 50, 281–290.

[38] Aiad, I., El-Didamony, H., Heikal, M., & Al-Masry, S. (2013) Effect of delaying addition time of synthesized SSPF condensate on the durability of sulphate resisting cement pastes incorporating micro-silica. Construction and Building Materials, 48, 1092–1103.

[39] Heikal, M., Ali, A. I., Ismail, M. N., & Ibrahim, S. A. N. (2014). Behavior of composite cement pastes containing silica nano-particles at elevated temperature. Construction and Building Materials, 70, 339–350.

[40] ASTM C109. Strength test method for compressive strength of hydraulic cement mortars; 2007.

[41] Liao, K. Y., Chang, P. K., Peng, Y. N., & Yang, C. C. (2004). AStudy on characteristics of interfacial transition zone in concrete. Cement and Concrete Research, 34(6), 977-989.

[42] Hakamy, A., Shaikh, F.U.A., & Low, I. M. (2015). Effect of calcined nanoclay on microstructural and mechanical properties of

chemically treated hemp fabric-reinforced cement nanocomposites. Construction and Building Materials, 95, 882-891.
[43] Aleem, S. A. E., Heikal, M., & Morsi, W. M. (2014). Hydration characteristics, thermal expansion and microstructure of cement pastes and mortars containing nano SiO_2. Construction and Building Materials, 59, 151–160.
[44] Heikal, M., Abd El Aleem, S., & Morsi, W. M. (2013). Characteristics of blended cements containing nano-silica. HBRC Journal, 9 (3), 243–255.
[45] Abbas, R., Abo-El-Enein, S. A., & Ezzat, E. S. (2010). Properties and durability of metakaolin blended cements: Mortar and concrete. Materiales De Construccion, 60 (300), 33–49.
[46] Said-Mansour, M., Kadri, E. H., Kenai, S., Ghrici, M., & Bennaceur, R. (2011). Influence of calcined kaolin on mortar properties, Construction and building Materials, 25(5), 2275–2282.
[47] Alonso, C., & Fernandez, L. (2004). Dehydration and rehydration processes of cement paste exposed to high temperature environments. Journal of materials science, 39(9), 3015–3024.
[48] Aiad, I., El-Didamony, H., Heikal, M., &Al-Masry, S. (2013). Effect of delaying addition time of synthesized SSPF condensate on the durability of sulphate resisting cement pastes incorporating micro-silica. Construction and Building Materials, 48, 1092–1103.
[49] El-Didamony, H., Aiad, I., Heikal, M., & Al-Masry, S. (2014). Impact of delayed addition time of SNF condensate on the fire resistance and durability of SRC–SF composite cement pastes. Construction and Building Materials, 50, 281–290.
[50] Walters, G. V., & Jones, T. R. (1991). Effect of metakaolin on alkali-silica reaction (ASR) in concrete manufactured with reactive aggregate durability of concrete. Special Publication, 126, 941-954.
[51] Piasta, J., Sawicz, Z., & Rudzinski, L. (1984). Changes in structure of hardened cement pastes due to high temperature. Materials Structure, 17(4), 291–296.
[52] Chan, Y. N., Peng, G. F., & Anson, M. (1999). Residual strength and pore structure of high strength concrete and normal strength concrete after exposure to high temperatures. Cement and concrete composites, 21(1), 23–27.
[53] Heikal, M. (2008). Effect of elevated temperature on the physico-mechanical and microstructural properties of blended cement pastes. Building Research Journal, 56(2), 157–172.
[54] Komonen, J., & Renttala, V. (2003). Effect of high temperature on the pore structure and strength of plain and polypropylene fiber reinforced cement pastes. Fire technology, 39(1), 23–34
[55] Heikal, M. (2000). Effect of temperature on the physico-mechanical and mineralogical properties of Homra pozzolanic cement pastes. Cement and Concrete Research, 30(11), 1835–1839.
[56] Heikal, M. (2006). Effect of temperature on structure and strength properties of cement pastes containing fly ash in combination with limestone. Ceramics-Silikaty, 50(3),167.
[57] Heikal, M., El- Didamony, H., Sokkary, T.M., & Ahmed, I. A. (2013). Behavior of composite cement pastes containing microsilica and fly ash at elevated temperature. Construction and building materials, 38, 1180–1190.